CHEMISTRY OF MATERIALS

pubs.acs.org/cm

Article

Postsynthetic Framework Contraction Enhances the Two-Photon Absorption Properties of Pillar-Layered Metal−Organic Frameworks

David C. Mayer,[‖] Jan K. Zaręba,[‖] Gabriele Raudaschl-Sieber, Alexander Pöthig, Marta Chołuj, Robert Zaleśny,* Marek Samoć,* and Roland A. Fischer*

Cite This: *Chem. Mater.* 2020, 32, 5682−5690

Read Online

ACCESS | Metrics & More | Article Recommendations | Supporting Information

ABSTRACT: Aggregation-induced emission (AIE) dyes have been shown to be a potential ligand class for multiphoton absorbing metal−organic frameworks (MPA-MOFs); however, the influence of framework flexibility on the local ligand conformation and its ramifications on the nonlinear absorption properties of this material class have sparsely been understood. In this study, we systematically investigate the two-photon absorption properties of two pillar-layered MOFs comprising tetraphenylethylene AIE ligands and compare the results to the organic ligand in crystal form, using a combination of linear and nonlinear optical characterization methods and electronic-structure calculations. We demonstrate that self-confining the AIE ligand is key to enhance the nonlinear optical absorption properties, as a structure transformation to contracted frameworks strongly increases the two-photon absorption response, which can be addressed by specific ligand substitution. Our results have important implications on the design of MPA-MOFs and provide synthetic guidelines not only from a fundamental point of view but also application-wise.

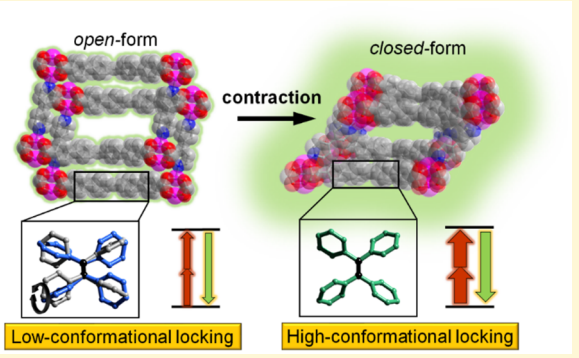

INTRODUCTION

Aggregation of molecules into dense phases can change their optical properties in manifold ways. Most organic and organometallic compounds feature high fluorescence quantum yields only in solutions of low concentration, whereas their emission properties deteriorate in solutions of higher concentration and/or almost completely disappear in the solid state. This phenomenon, referred to as concentration quenching or aggregation-caused quenching (ACQ), is the result of the formation of nonemissive states that may emerge for certain aggregation modes of aromatic chromophores. Undoubtedly, the ACQ effect is a major impediment to a number of applications of metal−organic framework (MOF)-based fluorophores such as fluorescence sensing and a significant obstacle when applications of MOFs are considered relying on two-photon-induced fluorescence.

On the other hand, Tang et al. found in 2001 that some classes of chromophores reveal an effect that is opposite to ACQ; i.e., certain groups of chromophores are highly emissive in the aggregated state, while their solutions reveal a very weak fluorescence.[1] This phenomenon, whose name was coined as aggregation-induced emission (AIE) or crystallization-induced emission (CIE), has sparked enormous interest due to potential applications in sensory studies of bioanalytes,[2] bioimaging,[3,4] and optoelectronics such as OLED devices.[5] The fundamental mechanism that lies behind increased quantum yields of aggregated molecules was found to originate from the reduction of nonradiative relaxation pathways such as the restriction of intramolecular vibrational and rotational motions.[6,7]

The incorporation of an AIE-active ligand, e.g., based on a tetraphenylethylene (TPE) scaffold into a coordination polymer (CP), appears to be an obvious strategy that allows one to suppress the above molecular motions in a conceptually similar manner as self-aggregation does. Indeed, the application of AIE-active ligands as building units of crystalline coordination networks (CCNs) has already gathered broad interest in the field.[8,9] For instance, a number of luminescent MOFs (LMOFs) as potential light phosphors or chemical sensors have been investigated combining high porosity and fluorescence quantum yield.[10,11] Also, detailed analysis of the underlying mechanism of fluorescence enhancement in TPE-based CPs has been conducted, and important descriptors were described, governing the linear photophysics of this kind of material.[9,12,13]

Our group was among the first to study the nonlinear optical properties of highly emissive MOFs composed of AIE ligands.

Received: April 2, 2020
Revised: June 9, 2020
Published: June 9, 2020

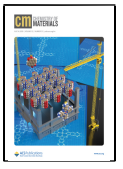

https://dx.doi.org/10.1021/acs.chemmater.0c01417
Chem. Mater. 2020, 32, 5682−5690

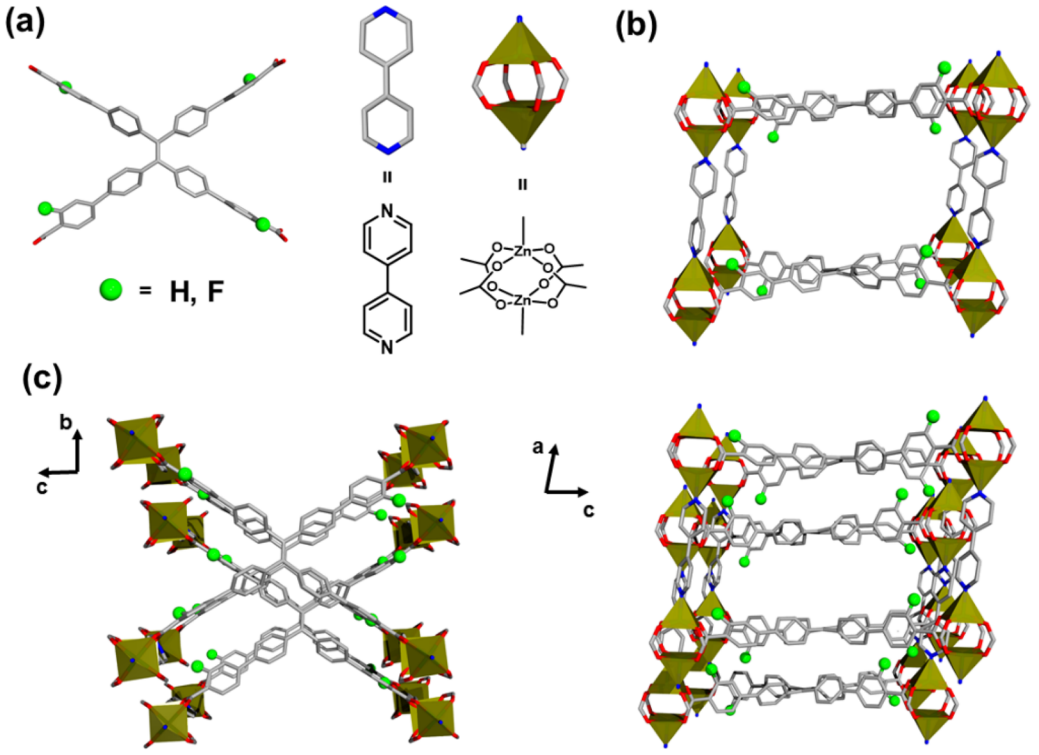

Figure 1. (a) Depiction of the building blocks for the synthesis of $[Zn_2(X)(bpy)]$ (**1**, X = **TCPE**; **1-F**, X = **TCPE-F**). (b) Single cavity of the **fsc** subframework composed of $[Zn_2(X)]_\infty$ grids connected by the bipyridine pillar. (c) View along the crystallographic *a*- and *b*-axes showing the 2-fold interpenetrated structures illustrating the chromophore distances ∼6 Å (between subframeworks) and ∼14 Å (within one framework).

We studied indium (In-MOF)- and zinc (Zn-MOF)-based MOFs incorporating (tetrakis[4-((4-carboxylato)phenyl)-phenyl]ethylene) (hereafter referred to as **H_4TCPE**), both capable of stimulated emission with low-threshold powers.[14] The enhanced MOF emission properties were not limited to the one-photon domain—characterizations of two-photon absorption (2PA) properties have shown that the values of the two-photon brightnesses were equal to 3072 GM (In-MOF) and 1053 GM (Zn-MOF, 1 GM = 10^{-50} cm^4 s $photon^{-1}$, named after German scientist Maria Göppert-Mayer), respectively, whereas for the parent ligand the corresponding value was equal to only 55 GM. The huge difference between those values in favor of MOFs demonstrated that incorporation of a ligand featuring AIE characteristics into CCNs can significantly increase its two-photon response. We also recently reported hafnium and zirconium MOFs based on the **H_4TCPE** ligand, whose nonlinear responses reached values as high as 3600 GM, likewise improved versus the bare ligand.[15] Electronic structure calculations performed at the time-dependent density functional theory (TD-DFT) level revealed a strong dependency on the conformational strain of the flexible ligand, as well as charge polarization of the latter by coordination to the metal-oxo-clusters. Very recently, Pan and co-workers reported a study on similar systems, concerning the pressure dependency of multiphoton absorption. The study in question demonstrated that external stimuli acting on flexible MOFs, composed of **TCPE** ligands, can dramatically enhance the MPA properties.[16]

Despite the data collected on 2PA of AIE-based MOFs so far, many open questions remain unaddressed regarding the limitations of this approach. Indeed, although the gathered data indicate that incorporation of AIE-based ligands into MOFs improves the 2PA properties, one needs to answer the question, is it really always the case? What about highly porous MOFs which are not capable of strong self-confinement of intramolecular vibrational and rotational motions of ligands? Will such MOFs still offer improved nonlinear response in comparison to free ligands, or will their response be deteriorated? More generally, to what extent is the flexibility of coordination networks our friend or foe in the search of maximized 2PA in coordination network compounds?

With such a set of delineated problems in mind, we embarked upon a study to explore the spectrally resolved 2PA properties of highly porous, isostructural pillar-layered MOFs, based on nonfluorinated and fluorinated TPE-AIE ligands (Figure 1), which additionally experience framework contraction upon removal of guest molecules. We structurally characterized the MOF materials and examined their wavelength-dependent 2PA properties for both the open and contracted frameworks. Together with density functional theory calculations, our results reveal that the MOFs studied in the present work provide inferior two-photon activity compared to the pure organic acids (**TCPE** and **TCPE-F**) in crystal form, but the two-photon activity can be restored by a contraction process, especially in the case of the MOF bearing a fluorinated ligand.

RESULTS AND DISCUSSION

Synthesis and Characterization of MOF Materials. Pillar-layered MOFs with the formal composition of $[Zn_2(X)(bpy)]$ (**1**, X = **TCPE**; **1-F**, X = **TCPE-F**) were obtained as yellow polycrystalline powders by solvothermal reaction of $Zn(NO_3)_2{\cdot}4\,H_2O$, **H_4TCPE** (**H_4TCPE-F**), and bpy [**H_4TCPE** = tetrakis[4-(4-carboxyphenyl)phenyl]ethylene, **H_4TCPE-F** = tetrakis[4-(4-carboxy-2-fluoro-phenyl)phenyl]ethylene, bpy =

https://dx.doi.org/10.1021/acs.chemmater.0c01417
Chem. Mater. 2020, 32, 5682−5690

4,4′-bipyridine] in dimethylformamide (DMF)/MeOH (1, 0.25) at 100 °C for 24 h following established literature protocols.[17,18] **1** and **1-F** were structurally characterized by single-crystal X-ray diffraction (SCXRD for **1**), powder X-ray diffraction (PXRD), Raman and infrared spectroscopy (IR), and solid-state NMR spectroscopy. Thermal stability was investigated by thermogravimetric analysis. SCXRD analysis shows that **1** and **1-F** are isostructural and isoreticular.

The MOFs crystallize in the triclinic space group $P\bar{1}$ and consist of zinc-based secondary building units (SBUs) in a paddlewheel geometry, which are connected by the **TCPE** (**TCPE-F**) ligand to form rectangular grids $[Zn_2(X)]_\infty$ (X = **TCPE**/**TCPE-F**). These grids are further linked together by the bpy pillars to give a pillar-layered structure in **fsc** topology. The rectangular $[Zn_2(X)]_\infty$ grids have a dimension of ∼16 × 20 Å, and the layers are separated by a distance of ∼14 Å with regard to each other. **1** and **1-F** are 2-fold interpenetrated, with the paddlewheel SBU of one subframework located near the edge of the second framework. The $[Zn_2(X)]_\infty$ grids of each subframework show distances of ∼6 Å. Despite interpenetration, the MOFs still contain ∼40% accessible void per unit cell. Note that **1-F** is also referred to as LMOF-301 and was initially synthesized by Li et al.[17] Structural evidence of the as-synthesized (solvated) MOFs **1** and **1-F** was proven by Pawley refinement, which is in good accordance with the results from SCXRD. Solvent exchange to acetone reveals a structural transformation of the MOFs, and further thermal activation (dynamic vacuum, 100 °C) finally leads to the loss of crystallinity. PXRD patterns of the solvent exchanged MOFs show the formation of a semicrystalline phase, which did not allow for satisfactory indexing of the unit-cell parameters (Figures S14 and S16), a commonly observed feature in pillar-layered MOFs.[18−20] The PXRD patterns, however, suggest a contracted framework, and neither **1** nor **1-F** is reforming after extensive impregnation of the MOFs with DMF solvent. Structural composition and framework contraction were further characterized by Raman and IR spectroscopy. The Raman spectra of **1** and **1-F** are dominated by signals from the ligands. The intensity of the ring breathing vibration mode (995 cm^{-1}) of the pyridine pillar is drastically reduced upon MOF incorporation, which reflects the coordination bond formation of the N-donor to the zinc paddlewheel SBU.[21] The Raman spectra of the activated MOFs, **1-contr** and **1-F-contr**, show no enhanced intensity of the pyridine ring breathing mode, supporting a framework contraction upon activation (Figures S35 and S36).[20] The IR spectra show the characteristic bands for coordinated **TCPE** (**TCPE-F**) and bpy.[22,23] Similar to the Raman spectroscopy results, the IR spectra show no formation of free organic acids nor 4,4′-bipyridine (Figures S31−S34), which demonstrates that the zinc paddlewheel SBU is preserved upon activation of the MOF materials. N_2 adsorption isotherms measured on the activated materials at 77 K indicate a low BET surface area (SA) of only 22 m^2/g for **1-contr** and 76 m^2/g for **1-F-contr**. The surface area values are far below theoretical values calculated based on the crystal structures of pristine MOFs (2332 and 2330 m^2/g, for **1** and **1-F**, respectively, see the Supporting Information), indicating evident structural deformation experienced upon activation. ^{13}C cross-polarized magic angle spinning solid-state (CPMAS) NMR spectra of solvated **1** and **1-F** prove the expected composition of the MOFs by showing the isotropic peaks for **TCPE** (**TCPE-F**) and bpy ligands.[9,24,25] The incorporated DMF was found with characteristic signals at 30, 35, and 162 ppm (Figures S8 and S10). Thermogravimetric analysis reveals a loss of incorporated DMF solvent up to 200 °C and MOF decomposition at ∼400 °C for **1**, (∼300 °C for **1-F**, Figures S23 and S24). Altogether, evaluation of the PXRD, IR, Raman, ^{13}C CPMAS NMR, and N_2 sorption analysis suggests that **1** and **1-F** undergo an irreversible structural deformation upon solvent exchange and subsequent activation, such that the MOF structures show a partial framework contraction (Figure 2), however with preserved network connectivity.[26,27] Solid-state absorbance spectroscopy supports our notion of a framework contraction of MOFs, as the absorbance spectra show a pronounced red-shift for both compounds of ∼50 nm, which is indicative of a change in the local environment of the **TCPE**/**TCPE-F** ligands (Figures S37 and S38).[20,28]

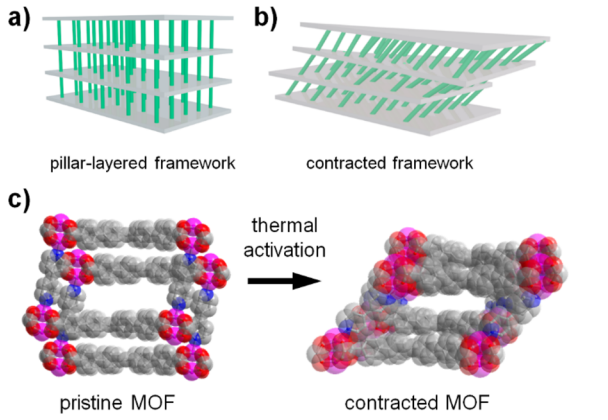

Figure 2. An illustration of structure transformations of pillar-layered frameworks. The pristine network (a) contracts with tilting pillars (b). (c) Sketch of MOF contraction in **1** and **1-F** upon solvent exchange and thermal activation.

When performing fluorescence measurements on the ligands and their corresponding MOFs, it was found that the fluorinated compounds are less bright than their non-fluorinated analogues, as well as that the MOFs are much less bright than the ligands. To quantify this, absolute quantum yield (φ) measurements with the use of an integration sphere were conducted. The determined φ values are 24.7%, 20.0%, 9.1%, and 6.9% for **TCPE**, **TCPE-F**, **1**, and **1-F**, respectively. The incorporation of **TCPE** and **TCPE-F** ligands into the respective MOFs renders over a 50% drop in φ. The contracted networks **1-contr** and **1-F-contr** feature enhanced φ values of 11.8% and 27.3%. Note the nearly 4-fold enhancement of φ for **1-F-contr** compared to **1-F**, and the relatively negligible enhancement in the case of **1-contr** compared to **1**. Moreover, steady-state and time-resolved one-photon spectroscopic studies of **TCPE**, **TCPE-F**, **1**, **1-F**, **1-contr**, and **1-F-contr** materials, presented in the SI, show that (i) contraction of MOFs results in the red-shift of their emission spectra; in the case of **1-F-contr** this effect is so strong that the emission envelope becomes nearly identical with that of **TCPE-F**. We take this as an indication that the geometry of ligands in **1-F-contr** and **TCPE-F** might be similar; (ii) the fluorescence decay lifetimes of as-synthesized MOFs are significantly lower than those of the corresponding solid ligands (see Figures S42 and S43 in the Supporting Information). Importantly, contraction of the MOF partially restores higher values of mean fluorescence lifetimes, mainly at longer emission wavelengths.

https://dx.doi.org/10.1021/acs.chemmater.0c01417
Chem. Mater. 2020, 32, 5682−5690

All the optical measurements attest to the fact that there is a common structural feature of **1** and **1-F** that has a negative impact on their one-photon spectroscopic properties. Given that **TCPE** and **TCPE-F** are AIE-active molecules, the observed differences in optical properties between the solid chromophores and MOFs most likely result from different degrees of restriction of molecular movements in those systems.[29] Similar findings have been described for MOFs incorporating TPE molecules with remarkable φ reduction due to low phenyl ring rotational barriers.[8,9,12,13,28,30−32]

To verify the hypothesis in question, the crystal structures of **TCPE** and **1** have been explored in terms of ligand dynamics. The projections of independent parts of their unit cells are provided in Figures S21 and S22, respectively. The crystal structure of **TCPE** comprises one **TCPE** acid molecule and one DMF molecule. The internal phenyl rings (TPE core) of **TCPE** are ordered. External phenyl rings (those connected to the carboxylic functional groups) feature elongated thermal displacement ellipsoids, which are not split into separate positions. Long axes of the thermal displacement ellipsoids are either parallel to the plane of the molecule, showing the presence of in-plane vibrations, or perpendicular to the plane of the benzoic acid subunit. It appears that, due to the tight packing of **TCPE** molecules in the crystal lattice, the phenylene fragments are prohibited from rotations. By contrast, the independent part of the unit cell of **1** shows a severely disordered **TCPE** molecule, along with two well-localized zinc ions and one ordered 4,4′-bipyridine molecule. The structural disorder of the **TCPE** molecule in **1** involves all phenylene rings of the TPE core and one external phenylene ring. The crystallographic model indicates that phenylene rings are rotationally disordered around their local C_2 axes over two positions with an occupancy ratio of 60:40.

To the best of our knowledge, the crystal structure of **TCPE-F** has not been reported yet. For this reason, an analogous structural comparison with **1-F** cannot be made. Nevertheless, a comparison of the ligand geometries in the investigated MOFs reveals that the disorder of the TPE core and one external phenylene ring in **1-F** is analogous to that of **1**, which means that the fluorine atoms exert minor intramolecular steric effects on the relative changes of ligand geometry in the case of the noncontracted networks (see Figure S22). Furthermore, looking into the type of intermolecular interactions between subframeworks in **1** and **1-F**, the crystal structures show the presence of several weak $\pi\cdots H-C_{arom}$ and $F\cdots H-C_{arom}$ interactions (characteristic distances from 2.09 to 2.84 Å).[33−38]

Altogether, the structure dynamics expressed by the high rotational disorder of TPE cores implies that in **1** and **1-F** the framework forces do not impart enough conformational strain to the AIE-active ligands (low conformational locking),[12] nor do intermolecular effects between subframeworks impact the ligand geometries (Figure 3). Consequently, the materials experience rotation-induced dissipation of excitation-energy,[39] similar to the free ligands in solution, quenching the emission properties to a large extent (Figure 3b). Note that phenyl ring flipping primarily increases the radiationless decay rate of the excited state in TPE.[7,40]

Nonlinear Optical Characterization. We further moved to the spectrally-resolved characterization of 2PA cross-sections with the use of the SSTPEF (solid-state two-photon excited fluorescence) method, see details in the SI.[41] The results show (Figure 4a) that the 2PA cross-sections for the solid ligand chromophores are the highest among all the materials investigated in this study, e.g., **TCPE** (476 GM, 670 nm) and **TCPE-F** (474 GM, 670 nm). It appears that **1** and

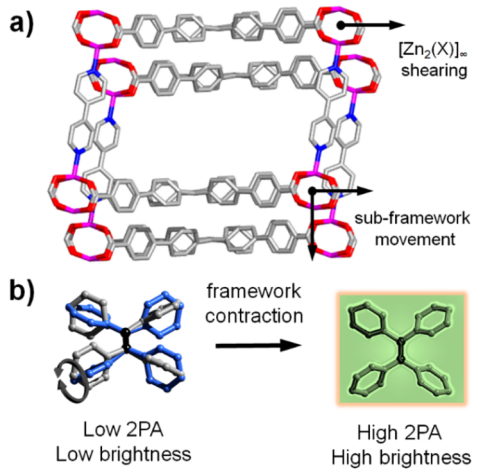

Figure 3. (a) Illustration of two probable modes present in the contraction of **1** and **1-F**: subframework movement or $[Zn_2(X)]_\infty$ shearing. (b) Rotation-induced excitation energy dissipation mechanism in TPE due to low conformational locking. Framework contraction enhances the latter and, similarly, enhances the one-photon and two-photon emission properties.

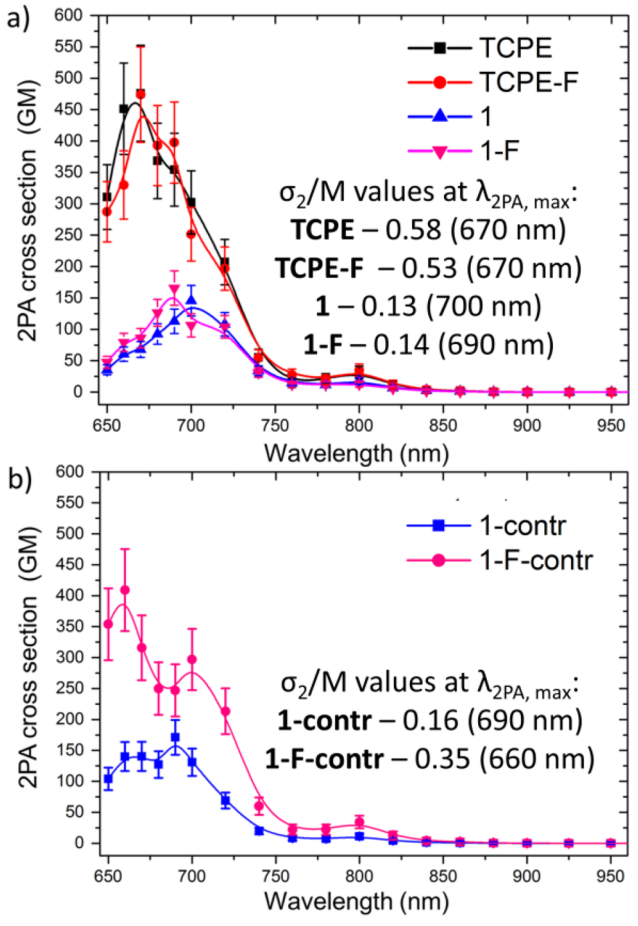

Figure 4. 2PA cross-sections determined for acids **TCPE** and **TCPE-F** and MOFs **1** and **1-F** (upper panel) and those for contracted networks **1-contr** and **1-F-contr** (lower panel). Lines are drawn to guide the eyes. The unit for σ_2/M is GM mol g^{-1}.

https://dx.doi.org/10.1021/acs.chemmater.0c01417
Chem. Mater. 2020, 32, 5682−5690

1-F feature much lower 2PA cross-sections than the corresponding ligands (145 GM at 700 nm and 165 GM at 690 nm, respectively; see Figure 4a). It should be stressed that the observed experimental relationships contrast our initial guess based on the previously investigated **TCPE**-based MOFs,[14−16] the most important of which is the surprising result of the *decrease* of 2PA activity upon incorporation of the ligands into the MOF, instead of its enhancement. Note also that the differences between two-photon responses of non-fluorinated and fluorinated analogues remain within their experimental errors; hence, it can be concluded that in these systems the fluorine substituent has a minor effect on the 2PA process. Molar mass-normalized merit factors[42] (σ_2/M) even more emphasize that the two-photon response of **1** and **1-F** is *worsened* in comparison to the two-photon response of the parent ligands **TCPE** and **TCPE-F**. Indeed, the merit factors show that there is around a 3-fold drop in the 2PA response of **1** and **1-F** in comparison to the neat chromophores (Figure 4b).

In addition, we have performed SSTPEF measurements also on the contracted networks **1-contr** and **1-F-contr**. Interestingly, one notes a large enhancement of the 2PA cross-section for **1-F-contr** compared to **1-F** (409 GM at 660 nm vs 165 GM at 690 nm), whereas little enhancement is observed for the pair of **1-contr** and **1** (171 GM at 690 nm vs 145 GM at 700 nm). Apparently, the fluorine substituent offers a large benefit as an additional tool for ligand dynamics suppression, however, only within the contracted MOF. It is evident that a particular improvement of one- and two-photon properties has been achieved for **1-F-contr** due to steric bulk imparted by the fluorine substituent. Accordingly, framework contraction does improve the one-photon emission parameters such as quantum yield and luminescence decay lifetimes (Figures S42 and S43) and offers enhancement of the 2PA cross-section. From the viewpoint of applications of CPs relying on the 2PA-induced fluorescence (e.g., NLO imaging or sensing) such a combination of photophysical effects is extremely advantageous,[43] as it enhances both terms contributing to the two-photon brightness ($\varphi\sigma_2$) of the 2PA-induced fluorescence. Indeed, if this merit factor is considered, the enhancement of the $\varphi\sigma_2$ value due to contraction is over 6-fold for **1-F**.

Electronic-Structure Calculations. Up to this point, the presented experimental evidence suggests that ligand conformation in the investigated systems might have a large impact on their 2PA properties; thus, to unveil the origins of the observed relationships in the experimental nonlinear absorption spectra, we have performed electronic-structure calculations using time-dependent density functional theory (with the aid of long-range-corrected CAM-B3LYP functional and the 6-31+G(d) basis set).[44,45] To that end, we have selected several geometries of organic ligands, extracted from the available crystallographic data for **TCPE** acid and MOFs **1** and **1-F**. The former one provides a well-defined conformation of the **TCPE** molecule in the pure, solid-state form, whereas the latter two MOF crystal structures inform us about conformations of disordered **TCPE** and **TCPE-F** units being a part of the coordination networks. As we have pointed out in the previous sections, the crystal structure of **TCPE-F** is not known. Hence, to enable comparisons between **TCPE** and **TCPE-F** molecules, the structure of the latter was assumed to be analogous to that of **TCPE**, but with hydrogen atoms at the *meta* position being replaced by fluorine ones. We are aware that such a procedure might not provide an exact reflection of the real conformation of **TCPE-F** in its crystal lattice, but it allows for a proper modeling of the fluorine effect on 2PA properties.

Electronic-structure calculations of 2PA cross-sections of **TCPE** and **TCPE-F** (conformations according to the solid-state conformers) corroborate the experimental finding that these ligands exhibit similar values of the 2PA cross-section (Tables S4 and S5 in the Supporting Information). In fact, we note almost identical values of this property for the two structures, which shows that the electronic effect exerted by fluorine atoms is minor and does not lead to the increase of the 2PA cross-section. The results of the calculations also demonstrate that the $S_0 \rightarrow S_1$ transition is two-photon-forbidden, but the corresponding one-photon oscillator strength is very high (Tables S4 and S5). On the other hand, the two-photon-allowed $S_0 \rightarrow S_2$ transition has a significant absorption cross-section and corresponds to the absorption feature seen at ca. 660 nm in the experimental two-photon spectra.

Next, we aimed to shed light on the striking experimental result of much lower 2PA responses of **1** and **1-F** MOFs vs the parent ligands. For both MOFs, we have performed electronic-structure calculations for the two limiting conformations that are found by X-ray crystallography as disordered parts (denoted as **A** and **B**, Figure 5 and Figure S22).

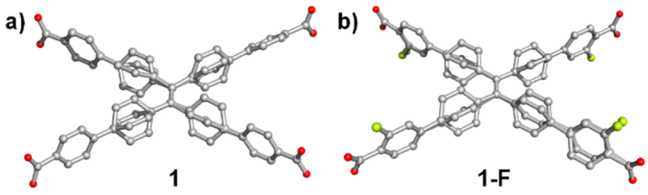

Figure 5. Depiction of the rotationally disordered parts in **1** (a) and **1-F** (b) as determined by SCXRD in the solid state. Carbon = gray, oxygen = red, fluorine = yellow.

Moreover, to appreciate the dynamic nature of ring flipping, analogous calculations have been performed for intermediate structures obtained from linear transformations between conformations **A** and **B**. The collected results indicate that the highest 2PA cross-sections indeed feature the crystallography-derived geometries **A** and **B** for both MOFs, whereas the simulated intermediate structures are much less two-photon active at long wavelength $S_0 \rightarrow S_2$ transition, which is also probed experimentally (Figure S45). It can therefore be assumed that the bulk of the two-photon response of the MOFs is attributable to the conformations **A** and **B**, especially taking into account their dominating participation in the disordered structures. With this in hand, we have compared 2PA cross-sections at maxima of **TCPE** and **1(A, B)**, and **TCPE-F** and **1-F(A, B)**. It turns out that in the case of the $S_0 \rightarrow S_2$ transition the corresponding values of the 2PA cross-sections for **A**/**B** geometries (Tables S6−S9 in the Supporting Information) are significantly smaller (2−3 times) than those for **TCPE** and **TCPE-F** (Tables S4 and S5). Noteworthy, a comparison of 2PA cross-sections of **TCPE** ligands within **1** and **1-F** MOFs does not reveal any significant influence of the fluorine atom on the 2PA properties, which again stays in agreement with SSTPEF measurements and is in line with theoretical and experimental results on the pair of the parent ligands **TCPE** and **TCPE-F**.

https://dx.doi.org/10.1021/acs.chemmater.0c01417
Chem. Mater. 2020, 32, 5682−5690

The experimental determination of the geometry of the **TCPE**/**TCPE-F** ligands in the contracted networks **1-contr** and **1-F-contr** is not possible given their amorphous nature, and this poses a serious obstacle for electronic-structure calculations of the effects of MOF contraction on 2PA values. On the other hand, spectroscopic similarities of the contracted networks to their parent ligands suggest that one of the effects of MOF contraction is that the ligand geometry is modified from a MOF-like to a purer ligand-like conformation. Hence, we here propose a synthetic approach in which we perform linear transformations between **1A** and **1B** geometries and **TCPE**, i.e., **1A** → **TCPE** and **1B** → **TCPE**. The results of the one- and two-photon spectra calculations are shown in Figures S45−S49. As it is seen, on passing from **1A** → **TCPE** and **1B** → **TCPE** there is a rise in the two 2PA cross-sections corresponding to the long-wavelength feature as a result of significant changes in the electronic structure (changes in excitation energies, transition moments, etc.) supporting a picture in which framework contraction indeed causes an increase of the 2PA activity of the MOFs.

While all those results allow us to confirm the observed relationships in the experimental data and relate specific ligand conformations with 2PA cross-sections, they do not indicate which specific electronic parameter is at the core of the observed changes. Accordingly, we have performed calculations using the three-state model[46] (see the SI for methodology), which allowed us to pinpoint the electronic-structure parameters that contribute to the strength of the dominant two-photon $S_0 \rightarrow S_2$ transition. We started from **TCPE** and **TCPE-F**, and we find that in both cases there is a dominant contribution from $|\mu^{01}||\mu^{12}|$ and $|\mu^{03}||\mu^{23}|$ products to two-photon $S_0 \rightarrow S_2$ transition strength (see eq S3 in the Supporting Information). In other words, the bright $S_0 \rightarrow S_1$ and $S_0 \rightarrow S_3$ one-photon excitations influence the strength of the two-photon $S_0 \rightarrow S_2$ transition (through corresponding $|\mu^{01}|$ and $|\mu^{03}|$ transition electric dipole matrix elements). It holds both for **TCPE** and **TCPE-F**, and one can thus conclude that similar 2PA properties of both species arise from alike electronic structures. Interestingly, the three-state model calculations reveal that the two-photon $S_0 \rightarrow S_2$ transition has a different character (in terms of excited-state contributions, as given by perturbation-theory expressions; see eq S1 in the Supporting Information) in the case of **1A** and **1B**. Namely, for the former structure the electronic $S_0 \rightarrow S_1$ excitation influences the two-photon $S_0 \rightarrow S_2$ transition intensity, while for the latter structure higher-lying states (S_3, S_4, and S_5) become important for the two-photon $S_0 \rightarrow S_2$ transition intensity. The important role of the S_1 state in the two-photon $S_0 \rightarrow S_2$ transition intensity is also found for all intermediate structures on the **1A** → **TCPE** transformation.

The large contribution of bright $S_0 \rightarrow S_1$ and $S_0 \rightarrow S_3$ one-photon excitations to the strength of the two-photon $S_0 \rightarrow S_2$ transition, as revealed by the three-state model, also allows one to draw a conclusion concerning a more general design principle of two-photon absorbing MOFs based on **TCPE**-like ligands. That relationship shows that engineering of the two-photon response can be addressed by modification of structural parameters that directly target the increase of one-photon $S_0 \rightarrow S_1$ and $S_0 \rightarrow S_3$ oscillator strengths. In practice, we suggest that this can be achieved by the extension of the **TCPE** core, leading to higher electron density delocalization, but also that the goal can be met by decoration of the aromatic scaffold with electron donor and/or electron acceptor functional groups.

CONCLUSION

We demonstrated that the porosity of a coordination polymer can be a double-edged sword when it comes to the crystal engineering of MOFs with maximized 2PA and emission properties based on AIE-ligand. On one hand, porosity may serve as a rich source of many additional functionalities, such as hosting of guest molecules or framework flexibility, while on the other hand, it itself can be responsible for ligand dynamics that favors undesired nonradiative relaxation pathways. The adopted ligand conformations within the MOF frameworks **1** and **1-F** studied in the present work show decreased two-photon activity compared to the conformation of the pure organic acids (**TCPE** and **TCPE-F**) in crystal form. Indeed, the analyzed MOFs (in the pristine, noncontracted state) were significantly inferior compared to their parent ligands in terms of both one-photon optical properties (lower quantum yields, shorter luminescence decay lifetimes) as well as 2PA cross-sections.

We have further proposed that the contraction of MOFs even to a noncrystalline state serves as a pathway to counteract undesirable effects connected with unrestricted molecular movements of ligands in the highly porous MOF matrix. We demonstrated that framework contraction not only improves one-photon emission parameters but also may be employed for enhancement of the 2PA cross-section. A particular benefit from such a contraction procedure is obtained when the ligand possesses additional steric hindrance. Indeed, improvement of one- and two-photon properties has been achieved for the **1-F-contr** material owing to the additional steric hindrance that is introduced by the dangling fluorine substituent.

The simultaneous enhancement of one-photon and two-photon excited emission parameters can be extremely helpful from the viewpoint of applications relying on 2PA (e.g., bioimaging). Furthermore, the fact that partial amorphization of MOFs leads to an enhanced nonlinear response is prospective, as it disengages from possible drawbacks of postsynthetic treatments (e.g., working in cellular environments when MOFs are used as two-photon probes).

Finally, in the presented study the previous 2PA studies on TPE-based MOFs are relativized. However, our new data confirm that the underlying concept of 2PA enhancement via conformational locking of the TPE core still holds. Targeted framework contraction adds a new aspect in the structure−property relation of 2PA active AIE-MOFs, when it comes to the search of maximized nonlinear optical response. We highlight that crystallinity of a coordination network seems not to constitute an essential factor for optimizing the nonlinear optical properties of CPs.

EXPERIMENTAL SECTION

Synthesis. All chemicals were received from commercial suppliers. H_4TCPE and H_4TCPE-F were synthesized according to the literature procedure.[14,17] **1** and **1-F** were prepared according to a published procedure,[17,18] but with a few modifications that are outlined in the Supporting Information. In short, 1 equiv of zinc nitrate tetrahydrate and 0.5 equiv of organic acids were dissolved in 2 mL of DMF. 1 equiv of 4,4′-bipyridine was dissolved in 0.5 mL of MeOH. The DMF mixture was smoothly covered with the methanolic pyridine solution and subsequently reacted at 100 °C for 24 h. Clear, yellow block crystals were collected via filtration.

https://dx.doi.org/10.1021/acs.chemmater.0c01417
Chem. Mater. 2020, 32, 5682−5690

Powder X-ray diffraction. Powder XRD patterns were obtained on a PANalytical Empyrean instrument equipped with a one-dimensional PIXCel-1D strip detector (Cu Kα_1 radiation, λ = 1.540 56 Å). Powders were measured in transmission geometry with the X-ray tube working at 40 kV and 40 mA.

Single-Crystal X-ray Diffraction. Single-crystal X-ray diffraction experiments were carried out on a Bruker D8 Venture diffractometer equipped with a Helios optic monochromator, a Photon 100 CMOS detector, and a Mo TXS rotating anode as source (Mo Kα radiation, λ = 0.7103 Å). The raw data were integrated using SAINT, and multiscan absorption correction was applied using SADABS within APEX3. The structure was solved by intrinsic phasing in SHELXT and refined in SHELXL. Hydrogen atoms were calculated in ideal positions using a riding model.

Thermogravimetric Analysis. TGA traces were measured on a TGA/DSC device from Mettler Toledo at a heating rate of 10 K/min in the temperature range 30−1000 °C using synthetic air as purging gas.

Raman and IR Studies. Raman spectra were collected on single-crystals using a Renishaw inVia Raman Microscope equipped with a diode laser operating at 785 nm excitation for both the contracted and noncontracted MOFs. IR spectra were recorded on a Frontier FT-IR spectrometer, which was placed inside a glovebox to enable measurements of activated samples.

Solid-State NMR Studies. ^{13}C CPMAS NMR measurements were conducted on a Bruker Avance 300 NMR device operating at 7.04 T with resonance frequency of 74.468 MHz for ^{13}C. The samples were packed in 2.5 mm using ZrO_2 rotors and measured at room temperature with rotational frequency of 30 kHz and a recycle delay of 2 s. Adamantane was used as an internal standard with a chemical shift of 29.472 ppm (CH group) referred to TMS.

Nitrogen Physisorption Measurements. Nitrogen isotherms were collected on a 3Flex surface characterization analyzer from Micromeritics at 77 K. Activated samples were outgassed prior to measurements using a Smart VacPrep sample preparation system. Pore-size distributions were obtained using DFT calculations with a N_2 cylindrical pores-oxide surface model.

Absorption, Steady-State, and Time-Resolved Photoluminescence Measurements. Solid-state absorbance and diffuse reflectance spectra were recorded on a SHIMADZU UV-3600 plus UV−vis NIR spectrophotometer equipped with a $BaSO_4$ coated integrating sphere detector. Fluorescence spectra were recorded with a fiber-coupled Ocean Optics 2000 CCD spectrograph using a picosecond laser diode operating at 377 nm. Spectrally resolved time-correlated single-photon counting emission lifetime measurements were performed on a Becker and Hickl system including a TCSPC module, a hybrid PMT detector mounted on a Princeton Instruments spectrograph. Excitation was delivered by a picosecond 377 nm laser diode.

Two-Photon Excited Fluorescence Measurements. A detailed description of the conducted measurements can be found in the Supporting Information. Nonlinear optical studies were performed using a laser system which consists of a Quantronix Integra-C regenerative amplifier operating as an 800 nm pump and a Quantronix-Palitra-FS BIBO crystal-based OPA. The system delivers tunable pulses of ∼130 fs length at a repetition rate of 1 kHz in the wavelength range 460−2000 nm. TPA studies were performed using the solid-state two-photon excited fluorescence (SSTPEF) technique. Prior to measurements the solid samples of H_4TCPE, H_4TCPE-F, **1**, **1-F**, **1-contr**, **1-F-contr**, and the reference compound (bis(4-diphenylamino)stilbene) were finely crushed and sieved using a set of mini-sieves to gain a crystal size smaller than 63 μm. The powders were fixed between microscope glass slides and mounted to a sample holder. The laser beam was directed onto samples at about 45°, while a set of collimating lenses, mounted to a glass optical fiber, were placed perpendicular to the plane of the sample. Scattered exciting radiation was removed using suitable short pass dielectric filters. The TPEF spectra were recorded by an Ocean Optics 2000 CCD spectrograph. The densities of all compounds, necessary for the calculation of two-photon brightnesses, were taken from crystallographic data.

■ ASSOCIATED CONTENT

Supporting Information

The Supporting Information is available free of charge at https://pubs.acs.org/doi/10.1021/acs.chemmater.0c01417.

Crystallographic data for **1** (CIF)

Instrumentation, synthetic procedures, powder X-ray diffraction data, ^{1}H NMR spectra, IR and Raman spectroscopy, TGA, adsorption isotherms, SS-NMR, linear optical and nonlinear optical characterization, and electronic structure calculations (PDF)

■ AUTHOR INFORMATION

Corresponding Authors

Robert Zaleśny − *Department of Physical and Quantum Chemistry, Faculty of Chemistry, Wroclaw University of Science and Technology, 50370 Wrocław, Poland;* orcid.org/0000-0001-8998-3725; Email: robert.zalesny@pwr.edu.pl

Marek Samoć − *Advanced Materials Engineering and Modelling Group, Wroclaw University of Science and Technology, 50370 Wrocław, Poland;* orcid.org/0000-0002-5404-2455; Email: marek.samoc@pwr.edu.pl

Roland A. Fischer − *Chair of Inorganic and Metal−Organic Chemistry, Department of Chemistry, Technical University of Munich, 85748 Garching, Germany;* orcid.org/0000-0002-7532-5286; Email: roland.fischer@tum.de

Authors

David C. Mayer − *Chair of Inorganic and Metal−Organic Chemistry, Department of Chemistry, Technical University of Munich, 85748 Garching, Germany*

Jan K. Zaręba − *Advanced Materials Engineering and Modelling Group, Wroclaw University of Science and Technology, 50370 Wrocław, Poland;* orcid.org/0000-0001-6117-6876

Gabriele Raudaschl-Sieber − *Chair of Inorganic and Metal−Organic Chemistry, Department of Chemistry, Technical University of Munich, 85748 Garching, Germany*

Alexander Pöthig − *Chair of Inorganic and Metal−Organic Chemistry, Department of Chemistry, Technical University of Munich, 85748 Garching, Germany;* orcid.org/0000-0003-4663-3949

Marta Chołuj − *Department of Physical and Quantum Chemistry, Faculty of Chemistry, Wroclaw University of Science and Technology, 50370 Wrocław, Poland;* orcid.org/0000-0003-2461-4851

Complete contact information is available at: https://pubs.acs.org/10.1021/acs.chemmater.0c01417

Author Contributions

‖D.C.M. and J.K.Z. contributed equally.

Notes

The authors declare no competing financial interest.

■ ACKNOWLEDGMENTS

The TUM is very greatly acknowledged for institutional funding. D.C.M. thanks the TUM Graduate School for financial support. We thank Pia Vervoorts for help with BET measurements. This research work was further supported by the DFG Priority Program 1928 "Coordination Networks: Building Blocks for Functional Systems" (www.coornets.de).

J.K.Z. is supported by the Foundation for Polish Science (FNP). J.K.Z. and M.S. acknowledge financial support from the Polish National Science Centre (NCN) under the Maestro 2013/10/A/ST4/00114 grant and from the Faculty of Chemistry, Wrocław University of Science and Technology. R.Z. and M.C. acknowledge financial support from the Polish National Science Centre (grant 2018/30/E/ST4/00457).

REFERENCES

(1) Hong, Y.; Lam, J. W. Y.; Tang, B. Z. Aggregation-induced emission. *Chem. Soc. Rev.* **2011**, *40* (11), 5361−5388.
(2) Kwok, R. T. K.; Leung, C. W. T.; Lam, J. W. Y.; Tang, B. Z. Biosensing by luminogens with aggregation-induced emission characteristics. *Chem. Soc. Rev.* **2015**, *44* (13), 4228−4238.
(3) Ding, D.; Li, K.; Liu, B.; Tang, B. Z. Bioprobes Based on AIE Fluorogens. *Acc. Chem. Res.* **2013**, *46* (11), 2441−2453.
(4) Qin, W.; Ding, D.; Liu, J.; Yuan, W. Z.; Hu, Y.; Liu, B.; Tang, B. Z. Biocompatible Nanoparticles with Aggregation-Induced Emission Characteristics as Far-Red/Near-Infrared Fluorescent Bioprobes for In Vitro and In Vivo Imaging Applications. *Adv. Funct. Mater.* **2012**, *22* (4), 771−779.
(5) Mei, J.; Leung, N. L. C.; Kwok, R. T. K.; Lam, J. W. Y.; Tang, B. Z. Aggregation-Induced Emission: Together We Shine, United We Soar! *Chem. Rev.* **2015**, *115* (21), 11718−11940.
(6) Zhao, Z.; Lam, J. W. Y.; Tang, B. Z. Tetraphenylethene: a versatile AIE building block for the construction of efficient luminescent materials for organic light-emitting diodes. *J. Mater. Chem.* **2012**, *22* (45), 23726−23740.
(7) Prlj, A.; Došlić, N.; Corminboeuf, C. How does tetraphenylethylene relax from its excited states? *Phys. Chem. Chem. Phys.* **2016**, *18* (17), 11606−11609.
(8) Shustova, N. B.; McCarthy, B. D.; Dincă, M. Turn-On Fluorescence in Tetraphenylethylene-Based Metal−Organic Frameworks: An Alternative to Aggregation-Induced Emission. *J. Am. Chem. Soc.* **2011**, *133* (50), 20126−20129.
(9) Shustova, N. B.; Ong, T.-C.; Cozzolino, A. F.; Michaelis, V. K.; Griffin, R. G.; Dincă, M. Phenyl Ring Dynamics in a Tetraphenylethylene-Bridged Metal−Organic Framework: Implications for the Mechanism of Aggregation-Induced Emission. *J. Am. Chem. Soc.* **2012**, *134* (36), 15061−15070.
(10) Hu, Z.; Lustig, W. P.; Zhang, J.; Zheng, C.; Wang, H.; Teat, S. J.; Gong, Q.; Rudd, N. D.; Li, J. Effective Detection of Mycotoxins by a Highly Luminescent Metal−Organic Framework. *J. Am. Chem. Soc.* **2015**, *137* (51), 16209−16215.
(11) Wang, F.-M.; Zhou, L.; Lustig, W. P.; Hu, Z.; Li, J.-F.; Hu, B.-X.; Chen, L.-Z.; Li, J. Highly Luminescent Metal−Organic Frameworks Based on an Aggregation-Induced Emission Ligand as Chemical Sensors for Nitroaromatic Compounds. *Cryst. Growth Des.* **2018**, *18* (9), 5166−5173.
(12) Shustova, N. B.; Cozzolino, A. F.; Dincă, M. Conformational Locking by Design: Relating Strain Energy with Luminescence and Stability in Rigid Metal−Organic Frameworks. *J. Am. Chem. Soc.* **2012**, *134* (48), 19596−19599.
(13) Shustova, N. B.; Cozzolino, A. F.; Reineke, S.; Baldo, M.; Dincă, M. Selective Turn-On Ammonia Sensing Enabled by High-Temperature Fluorescence in Metal−Organic Frameworks with Open Metal Sites. *J. Am. Chem. Soc.* **2013**, *135* (36), 13326−13329.
(14) Medishetty, R.; Nalla, V.; Nemec, L.; Henke, S.; Mayer, D.; Sun, H.; Reuter, K.; Fischer, R. A. A New Class of Lasing Materials: Intrinsic Stimulated Emission from Nonlinear Optically Active Metal−Organic Frameworks. *Adv. Mater.* **2017**, *29* (17), 1605637.
(15) Medishetty, R.; Nemec, L.; Nalla, V.; Henke, S.; Samoć, M.; Reuter, K.; Fischer, R. A. Multi-Photon Absorption in Metal−Organic Frameworks. *Angew. Chem., Int. Ed.* **2017**, *56* (46), 14743−14748.
(16) Chen, C.-X.; Yin, S.-Y.; Wei, Z.-W.; Qiu, Q.-F.; Zhu, N.-X.; Fan, Y.-N.; Pan, M.; Su, C.-Y. Pressure-Induced Multiphoton Excited Fluorochromic Metal−Organic Frameworks for Improving MPEF Properties. *Angew. Chem., Int. Ed.* **2019**, *58* (40), 14379−14385.
(17) Wang, F.; Liu, W.; Teat, S. J.; Xu, F.; Wang, H.; Wang, X.; An, L.; Li, J. Chromophore-immobilized luminescent metal−organic frameworks as potential lighting phosphors and chemical sensors. *Chem. Commun.* **2016**, *52* (67), 10249−10252.
(18) Tao, Ch.; Ying, Y.; Wang, H.; Chen, B.; Zhu, G.; Song, Y.; Liu, X.; Zhao, Z.; Shen, L.; Tang, B. Z. Nonwoven fabric coated with a tetraphenylethene-based luminescent metal-organic framework for selective and sensitive sensing of nitrobenzene and ammonia. *J. Mater. Chem. C* **2018**, *6* (45), 12371−12376.
(19) Ma, B.-Q.; Mulfort, K. L.; Hupp, J. T. Microporous Pillared Paddle-Wheel Frameworks Based on Mixed-Ligand Coordination of Zinc Ions. *Inorg. Chem.* **2005**, *44* (14), 4912−4914.
(20) Qi, Y.; Xu, H.; Li, X.; Tu, B.; Pang, Q.; Lin, X.; Ning, E.; Li, Q. Structure Transformation of a Luminescent Pillared-Layer Metal−Organic Framework Caused by Point Defects Accumulation. *Chem. Mater.* **2018**, *30* (15), 5478−5484.
(21) Kumari, G.; Patil, N. R.; Bhadram, V. S.; Haldar, R.; Bonakala, S.; Maji, T. K.; Narayana, C. Understanding guest and pressure-induced porosity through structural transition in flexible interpenetrated MOF by Raman spectroscopy. *J. Raman Spectrosc.* **2016**, *47* (2), 149−155.
(22) Zeleňák, V.; Vargová, Z.; Györyová, K. Correlation of infrared spectra of zinc(II) carboxylates with their structures. *Spectrochim. Acta, Part A* **2007**, *66* (2), 262−272.
(23) Tan, K.; Nijem, N.; Canepa, P.; Gong, Q.; Li, J.; Thonhauser, T.; Chabal, Y. J. Stability and Hydrolyzation of Metal Organic Frameworks with Paddle-Wheel SBUs upon Hydration. *Chem. Mater.* **2012**, *24* (16), 3153−3167.
(24) Hoffmann, H. C.; Debowski, M.; Müller, P.; Paasch, S.; Senkovska, I.; Kaskel, S.; Brunner, E. Solid-State NMR Spectroscopy of Metal−Organic Framework Compounds (MOFs). *Materials* **2012**, *5* (12), 2537−2572.
(25) Lucier, B. E. G.; Chen, S.; Huang, Y. Characterization of Metal−Organic Frameworks: Unlocking the Potential of Solid-State NMR. *Acc. Chem. Res.* **2018**, *51* (2), 319−330.
(26) ZareKarizi, F.; Joharian, M.; Morsali, A. Pillar-layered MOFs: functionality, interpenetration, flexibility and applications. *J. Mater. Chem. A* **2018**, *6* (40), 19288−19329.
(27) Dodson, R. A.; Wong-Foy, A. G.; Matzger, A. J. The Metal−Organic Framework Collapse Continuum: Insights from Two-Dimensional Powder X-ray Diffraction. *Chem. Mater.* **2018**, *30* (18), 6559−6565.
(28) Wei, Z.; Gu, Z.-Y.; Arvapally, R. K.; Chen, Y.-P.; McDougald, R. N.; Ivy, J. F.; Yakovenko, A. A.; Feng, D.; Omary, M. A.; Zhou, H.-C. Rigidifying Fluorescent Ligands by Metal−Organic Framework Formation for Fluorescence Blue Shift and Quantum Yield Enhancement. *J. Am. Chem. Soc.* **2014**, *136* (23), 8269−8276.
(29) Xiong, J.-B.; Feng, H.-T.; Sun, J.-P.; Xie, W.-Z.; Yang, D.; Liu, M.; Zheng, Y.-S. The Fixed Propeller-Like Conformation of Tetraphenylethylene that Reveals Aggregation-Induced Emission Effect, Chiral Recognition, and Enhanced Chiroptical Property. *J. Am. Chem. Soc.* **2016**, *138* (36), 11469−11472.
(30) Zhang, Q.; Su, J.; Feng, D.; Wei, Z.; Zou, X.; Zhou, H.-C. Piezofluorochromic Metal−Organic Framework: A Microscissor Lift. *J. Am. Chem. Soc.* **2015**, *137* (32), 10064−10067.
(31) Banerjee, D.; Hu, Z.; Li, J. Luminescent metal−organic frameworks as explosive sensors. *Dalton Trans.* **2014**, *43* (28), 10668−10685.
(32) Ma, L.; Feng, X.; Wang, S.; Wang, B. Recent advances in AIEgen-based luminescent metal−organic frameworks and covalent organic frameworks. *Mater. Chem. Front.* **2017**, *1* (12), 2474−2486.
(33) Samie, A.; Salimi, A.; Garrison, J. C. Exploration of relative π-electron localization in naphthalene aromatic rings by C−H···π interactions: experimental evidence, computational criteria, and database analysis. *CrystEngComm* **2019**, *21* (42), 6432−6445.
(34) Nishio, M. CH/π hydrogen bonds in crystals. *CrystEngComm* **2004**, *6* (27), 130−158.
(35) Kuś, P.; Kusz, J.; Książek, M. Aromatic C−H···π, C−H···O and parallel aromatic−aromatic interactions in the crystal structure of

https://dx.doi.org/10.1021/acs.chemmater.0c01417
Chem. Mater. 2020, 32, 5682−5690

meso-tetrakis[4-(benzyloxy)phenyl]porphyrin. *J. Chem. Crystallogr.* **2020**, *50* (1), 21−27.
(36) Mocilac, P.; Osman, I. A.; Gallagher, J. F. Short C−H···F interactions involving the 2,5-difluorobenzene group: understanding the role of fluorine in aggregation and complex C−F/C−H disorder in a 2 × 6 isomer grid. *CrystEngComm* **2016**, *18* (30), 5764−5776.
(37) D'Oria, E.; Novoa, J. J. The nature of the C-H···F interaction found in molecular crystals evaluated by ab initio calculations. *Acta Crystallogr., Sect. A: Found. Crystallogr.* **2006**, *62* (a1), s168.
(38) Thalladi, V. R.; Weiss, H.-C.; Bläser, D.; Boese, R.; Nangia, A.; Desiraju, G. R. C−H···F Interactions in the Crystal Structures of Some Fluorobenzenes. *J. Am. Chem. Soc.* **1998**, *120* (34), 8702−8710.
(39) Le Bras, L.; Chaitou, K.; Aloïse, S.; Adamo, C.; Perrier, A. Aggregation-caused quenching versus crystallization induced emission in thiazolo[5,4-b]thieno[3,2-e]pyridine (TTP) derivatives: theoretical insights. *Phys. Chem. Chem. Phys.* **2019**, *21* (1), 46−56.
(40) Kokado, K.; Sada, K. Consideration of Molecular Structure in the Excited State to Design New Luminogens with Aggregation-Induced Emission. *Angew. Chem., Int. Ed.* **2019**, *58* (26), 8632−8639.
(41) Medishetty, R.; Zaręba, J. K.; Mayer, D.; Samoć, M.; Fischer, R. A. Nonlinear optical properties, upconversion and lasing in metal−organic frameworks. *Chem. Soc. Rev.* **2017**, *46* (16), 4976−5004.
(42) Schwich, T.; Cifuentes, M. P.; Gugger, P. A.; Samoc, M.; Humphrey, M. G. Electronic, Molecular Weight, Molecular Volume, and Financial Cost-Scaling and Comparison of Two-Photon Absorption Efficiency in Disparate Molecules (Organometallic Complexes for Nonlinear Optics. 48.) − A Response to "Comment on 'Organometallic Complexes for Nonlinear Optics. 45. Dispersion of the Third-Order Nonlinear Optical Properties of Triphenylamine-Cored Alkynylruthenium Dendrimers.' Increasing the Nonlinear Response by Two Orders of Magnitude. *Adv. Mater.* **2011**, *23* (12), 1433−1435.
(43) Olesiak-Banska, J.; Waszkielewicz, M.; Obstarczyk, P.; Samoc, M. Two-photon absorption and photoluminescence of colloidal gold nanoparticles and nanoclusters. *Chem. Soc. Rev.* **2019**, *48* (15), 4087−4117.
(44) Yanai, T.; Tew, D. P.; Handy, N. C. A new hybrid exchange−correlation functional using the Coulomb-attenuating method (CAM-B3LYP). *Chem. Phys. Lett.* **2004**, *393* (1), 51−57.
(45) Ditchfield, R.; Hehre, W. J.; Pople, J. A. Self-Consistent Molecular-Orbital Methods. IX. An Extended Gaussian-Type Basis for Molecular-Orbital Studies of Organic Molecules. *J. Chem. Phys.* **1971**, *54* (2), 724−728.
(46) Alam, M. M.; Chattopadhyaya, M.; Chakrabarti, S. Solvent induced channel inter- ference in the two-photon absorption process a theoretical study with a generalized few-state-model in three dimensions. *Phys. Chem. Chem. Phys.* **2012**, *14*, 1156−1165.

https://dx.doi.org/10.1021/acs.chemmater.0c01417
Chem. Mater. 2020, 32, 5682−5690